Food Control 191 (2027) 112448

Contents lists available at ScienceDirect

Food Control

journal homepage: www.elsevier.com/locate/foodcont

Integrating fluorescence microscopy and Generalized Additive Models to predict *Escherichia coli* colonization dynamics on lettuce leaves

Stefania Truschi [a], Marianna Arvaniti [b], Marco Napoli [a,*], Massimiliano Marvasi [c], Anna Lenzi [a], Panagiotis Skandamis [b]

[a] Department of Agriculture, Food, Environment and Forestry (DAGRI), University of Florence, Florence, 50144, Italy
[b] Laboratory of Food Quality Control and Hygiene, Department of Food Science and Human Nutrition, Agricultural University of Athens, Athens, Greece
[c] Department of Biology, University of Florence, Sesto Fiorentino, Florence, 50019, Italy

ARTICLE INFO

Keywords:
Fluorescence microscopy
Escherichia coli
Leaf surface morphology
Generalized additive models
Ready-to-eat salads

ABSTRACT

Leafy greens are susceptible to contamination by human pathogens, and because ready-to-eat salads cannot undergo thermal decontamination, even initial contamination poses a food safety risk. To understand early bacterial colonization, we combined high-resolution fluorescence microscopy with Generalized Additive Models (GAMs) to investigate development of *Escherichia coli* micro-colonies on the leaves of romaine lettuce (*Lactuca sativa* L. var. *longifolia*) and wild lettuce (*Lactuca serriola* L.). Green Fluorescent Protein labelled bacteria were used as experimental tracers to visualize colonization dynamics under controlled conditions. Bacterial proliferation was quantified through fluorescence area, representing spatial expansion, and fluorescence intensity, reflecting aggregation; their combined metric provided a reliable proxy for micro-colony development. Over the 24 h incubation period, romaine lettuce consistently supported higher colonization than wild lettuce, reflecting differences in leaf surface micro-morphology. Maximum surface roughness emerged as a structural factor associated with bacterial proliferation. GAMs captured nonlinear growth patterns and species-specific responses, with romaine models explaining up to 91% of the observed variance. Comparison with Colony Forming Units (CFU) counts showed that fluorescence imaging resolved early spatial aggregation and colony expansion, whereas CFU measurements assessed culturability but lost spatial information due to tissue homogenization. Although fluorescence imaging based on genetically labelled bacteria is not directly applicable to post-harvest monitoring, it provides a platform for establishing predictive relationships between leaf surface traits and microbial growth. GAMs represent the transferable outcome of the study, enabling quantitative evaluation of temporal and morphological predictors of colonization dynamics and supporting approaches for improving microbiological safety in fresh-cut salad production systems.

1. Introduction

Fresh vegetables, while generally considered healthy and safe, may occasionally host pathogenic microorganisms capable of causing severe infections (Lorenzo et al., 2018; Mishra et al., 2024; Sobhy et al., 2023), including *Salmonella enterica*, pathogenic *Escherichia coli, Shigella* spp., *Listeria monocytogenes*, *Klebsiella pneumoniae*, *Pseudomonas aeruginosa*, and *Staphylococcus aureus* (Beuchat, 2002; Qian et al., 2022; Roasto et al., 2023). In Western countries, numerous foodborne outbreaks have been linked to ready-to-eat (RTE) leafy salads, particularly lettuce. Between 2003 and 2012, the United States reported 390 *E. coli* O157:H7 outbreaks, many associated with minimally processed foods (Centers for Disease Control & & Prevention, 2022). Within this broader context, 40 outbreaks associated specifically with leafy greens were reported in the U.S. and Canada from 2009 to 2018, resulting in 1212 illnesses, 77 cases of hemolytic uremic syndrome, and 8 deaths (Marshall et al., 2020).

Since these products are consumed raw and cannot undergo thermal decontamination, any acquired pathogen poses a direct and severe health risk to consumers, making food safety management a critical challenge in the fresh-produce chain (Mir et al., 2018). Furthermore, the production of RTE salads involves several processing steps, including shredding, cutting, washing, and packaging (Ölmez, 2016), during which favorable conditions for microbial colonization and growth can arise, particularly due to mechanical damage of delicate tissues, the

* Corresponding author.
E-mail address: marco.napoli@unifi.it (M. Napoli).

https://doi.org/10.1016/j.foodcont.2026.112448
Received 30 April 2026; Received in revised form 27 June 2026; Accepted 3 July 2026
Available online 4 July 2026

release of intra-(plant) cellular content and the limited effectiveness of washing and disinfection procedures (Banach et al., 2015; Delaquis et al., 2007). Among leafy greens, romaine lettuce has repeatedly been implicated in large-scale outbreaks (Coulombe et al., 2020; Slayton et al., 2013; Taylor et al., 2013; Waltenburg et al., 2022), highlighting the importance of understanding plant-specific and cultivar-specific susceptibility to contamination.

Advancements in fluorescence microscopy and molecular labeling techniques have enhanced the ability to investigate plant–pathogen interactions in microscale. Previous studies have shown that *E. coli* O157:H7 and *S. enterica* preferentially colonize natural openings (e.g., stomata) and mechanically damaged regions (Brandl, 2009; Seo & Frank, 1999). Moreover, leaf surface properties, such as epicuticular wax structure, surface hydrophobicity, roughness, and stomatal density, strongly influence bacterial adhesion and colonization, spatial distribution and eventually persistence (Truschi et al., 2023, 2024). Notably, wild lettuce (*Lactuca serriola*) exhibits reduced susceptibility to colonization compared to cultivated types, largely due to its higher surface hydrophobicity and distinct wax crystal morphology (Truschi et al., 2024).

Despite these insights, current strategies for monitoring spatio-temporal dynamics of bacterial colonization on lettuce surfaces remain limited, relying mainly on colony-forming unit (CFU) counts, which are destructive, time-consuming, and fail to capture the spatial dynamics of early colonization processes. Biological colonization processes are inherently nonlinear because bacterial proliferation is influenced simultaneously by time and multiple interacting leaf surface properties. Consequently, statistical approaches capable of describing nonlinear relationships without imposing predefined functional forms are particularly well suited to investigate these complex interactions. Generalized Additive Models (GAMs) provide this flexibility while maintaining a high degree of interpretability (Wood, 2017). In this study, we propose an integrated fluorescence-based approach to track *E. coli* growth directly on lettuce surfaces using Green Fluorescent Protein (GFP)-labelled bacteria combined with a Generalized Additive Models (GAMs)-based statistical modeling framework. Here, GFP labeling was used as an experimental tracer to enable high-resolution quantification of colonization dynamics under controlled conditions rather than as a detection strategy applicable to post-harvest processing environments. Unlike conventional predictive microbiology models, which estimate bacterial population growth under defined environmental conditions, the proposed GAM framework was developed to quantify the relative contribution of incubation time and leaf surface micro-morphology to the spatial development of bacterial micro-colonies. Fluorescence microscopy enables high-resolution monitoring of both fluorescence area, reflecting spatial colonization, and fluorescence intensity, providing an indirect measure of bacterial aggregation density; GAMs provide a flexible statistical framework for describing nonlinear relationships between incubation time, leaf surface morphology, and fluorescence-derived descriptors of colonization, allowing the relative contribution of each predictor to be quantified without assuming predefined functional relationships.

Because intact lettuce leaves were unsuitable for quantitative high-resolution fluorescence imaging with the microscopy configuration adopted in this study, owing to their thickness and intrinsic autofluorescence, reliable visualization of individual bacterial cells and early micro-colony development was technically challenging. To overcome these limitations, bacterial colonization was monitored on isolated adaxial epidermal layers placed on gels prepared from leaf cellular extracts. This experimental configuration preserved the surface micro-morphology relevant to bacterial attachment while providing a thin, optically accessible system that enabled reproducible high-resolution fluorescence imaging of early colonization events.

The specific objectives of this work were: (i) to monitor the proliferation and spatial distribution of a GFP-labelled *E. coli* strain on baby leaves of cultivated lettuce, romaine type (*Lactuca sativa* L. var. Longifolia "Bionda degli Ortolani") and wild lettuce (*Lactuca serriola* L.); (ii) to assess the influence of incubation time and morphological traits on colonization dynamics; (iii) to develop and evaluate a GAM-based statistical framework describing the relationship between incubation time, leaf surface morphology and bacterial colonization dynamics. The experimental progression from plant cultivation and bacterial inoculation to subsequent fluorescence microscopy observations is structurally outlined in Fig. 1.

This methodological time-lapse-based framework provides quantitative insights into the impact of leaf surface morphology on spatio-temporal bacterial dynamics and proposes a predictive modeling approach that may support future development of non-destructive assessment strategies for microbiological risk assessment in fresh-cut produce systems.

2. Materials and methods

2.1. Plant material and growing conditions

Seeds of romaine lettuce 'Bionda degli Ortolani' (*Lactuca sativa* L.) (Fratelli Ingegnoli, Milan, Italy) hereafter RL, and wild lettuce (*Lactuca serriola* L.) (Provencemonamour, Paris, France), hereafter WL, were sown in pots (15 cm in diameter, 13 cm in height, 1.5 L in volume) filled with a peat-based growing medium, at a density of approximately 0.3 seeds cm^{-2}. After sowing, plants were transferred to a growth chamber at 22 ± 2 °C with a 16 h photoperiod under fluorescent lighting (CULTILITE HPS Lamp, 400W) and grown until the baby-leaf stage.

2.2. Preparation of plant juice-agar medium

Plant juice–agar media were prepared separately for each lattuce species to provide a hydrated and chemically representative substrate for bacterial colonization during fluorescence microscopy observations. Because the isolated epidermal layers used for imaging were detached from the underlying leaf tissues, the plant juice–agar medium was designed to reproduce the nutrient environment surrounding the epidermis while maintaining the optical transparency required for high-resolution fluorescence microscopy. This experimental configuration allowed bacterial colonization to be investigated under controlled conditions while preserving the native leaf surface architecture responsible for bacterial attachment. Transparent agar media have previously been employed to monitor bacterial colony development under controlled conditions (Arvaniti et al., 2024). Building on this concept, the present study extends the approach by combining species-specific plant juice–agar with isolated lettuce epidermal layers. This configuration simultaneously preserves the structural characteristics of the leaf surface and provides host-derived nutrients, thereby offering a biologically relevant platform for investigating early bacterial attachment and micro-colony development. In detail, the plant juice was prepared starting from 25 g of leaves grinded in 250 mL of Ringer's solution (Oxoid, UK). The mixture was homogenized using a hand mixer until a uniform suspension was obtained. Subsequently, the mixture was heat-treated at 80 °C for 30 min to inactivate endogenous enzymes while preserving the chemical composition of the extract, following an adaptation of a protocol previously developed for sterile fresh-produce extracts (Manios et al., 2013). Plant juice was stored at 4 °C for up to one week and then filtered through Whatman cellulose filter paper. After filtration, agar was added to obtain a final dilution of 1:5 (v/v). The plant juice-agar medium was mixed while heating, under continuous stirring, until it was brought to a brief boil, and then poured into Petri dishes (9 cm in diameter; 8 mL per dish).

2.3. Bacterial strain, inoculum preparation, and leaf contamination

GFP-labelled *Escherichia coli* S17-1 pHC60 (Cheng & Walker, 1998), kindly provided by the laboratory of Prof. Alessio Mengoni (University

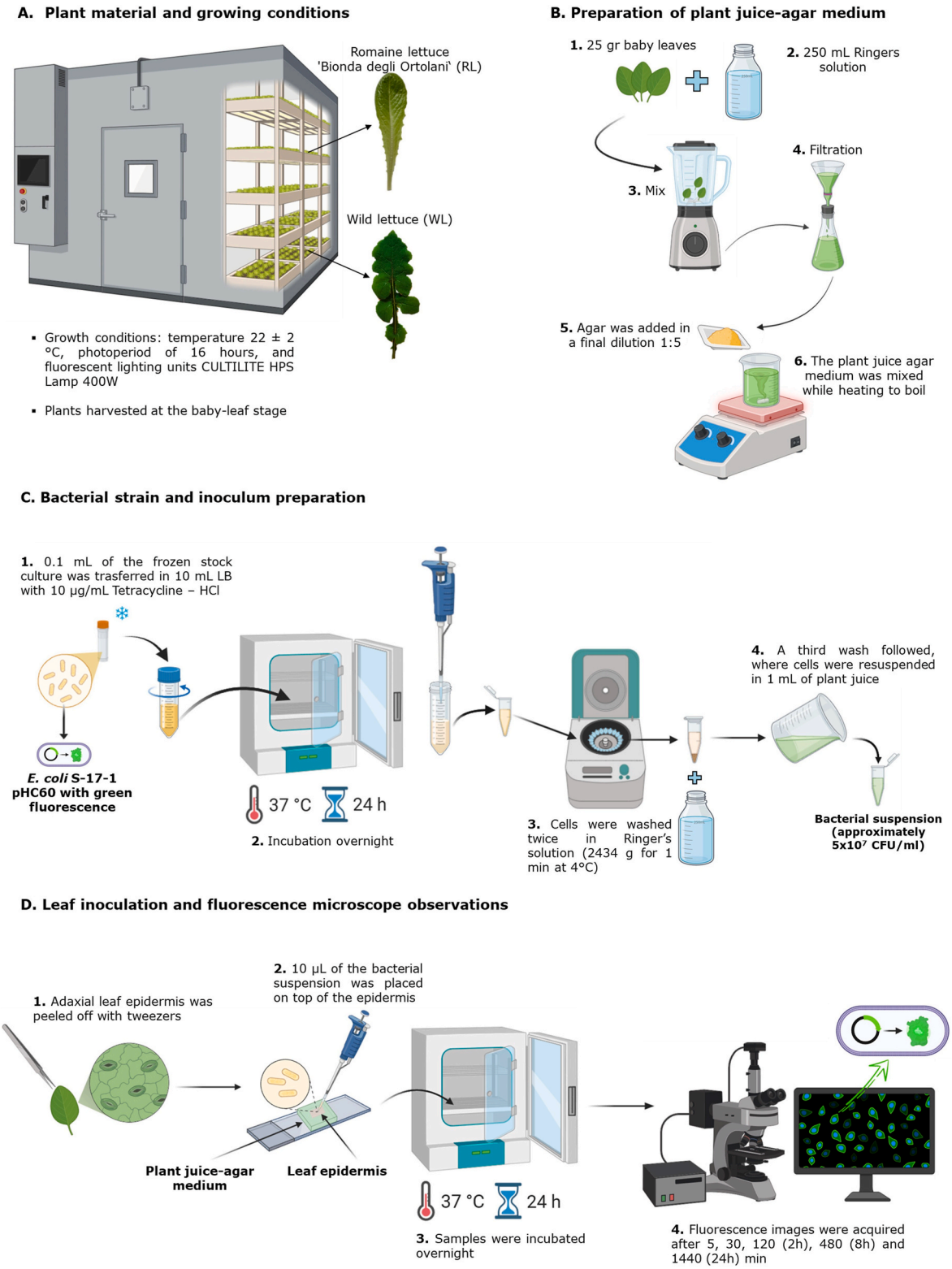

Fig. 1. The main steps from plant cultivation to bacterial inoculation and fluorescence microscopy observations.

of Florence), was used as the inoculum for leaf contamination assays. Working cultures were prepared from frozen stocks at −20 °C (Lysogeny Broth [LB, Oxoid, UK] with 10 µg mL^{-1} Tetracycline-HCl [Sigma-Aldrich] contaning 20% glycerol). An aliquot of 0.1 mL of the frozen stock culture was put in 10 mL LB with 10 µg mL^{-1} Tetracycline-HCl and incubated overnight at 37 °C. Cells were then washed twice in Ringer's solution (Oxoid, UK) to maintain the osmotic stability and harvested by centrifugation (2434 × *g* for 1 min at 4 °C), then resuspended in 1 mL of plant juice.

To enable reproducible high-resolution fluorescence imaging of early

bacterial colonization, the adaxial epidermis was carefully separated from intact leaves and transferred onto the corresponding plant juice–agar medium. Intact lettuce leaves were unsuitable for quantitative imaging at the required spatial resolution because their thickness and intrinsic autofluorescence reduced image quality and hindered reliable visualization of individual bacterial cells and developing micro-colonies (Donaldson, 2020). Isolation of the epidermis is a well-established approach for improving visualization of leaf surface micro-morphology while preserving the structural features relevant to surface interactions (Yuan et al., 2020).

Small 22 × 22 mm pieces of plant juice–agar medium prepared from the two species were cut and placed onto microscope slides. Ten microliters of Ringer's solution were placed onto each piece. The adaxial leaf epidermis of RL and WL was peeled off with tweezers and subsequently placed onto the plant juice–agar medium pieces. Finally, 10 μL of the bacterial suspension (approximately 5×10^7 CFU mL^{-1}) was applied on top of the epidermis. Samples were incubated at a constant temperature of 37 °C, corresponding to the optimal growth temperature for *E. coli*, for up to 1440 min (24 h).

2.4. Fluorescence microscopy and image analysis

An inverted fluorescence microscope (Leica, DMi8) equipped with an oil immersion 63× phase contrast objective, a DFC 7000T camera (Leica), and LAS X software (Leica) was used to monitor *E. coli* proliferation in RL and WL. Fluorescence images (view field: 197.5 μm × 148.1 μm) were acquired after 5, 30, 120 min (2 h), 480 min (8 h) and 1440 min (24 h) of incubation. The three images obtained by fluorescence microscopy, one of plant cells, one of the fluorescence signal, and one resulting from their overlap, are provided in Supplementary Fig. 1 for RL and Supplementary Fig. 2 for WL. During observation, the samples were covered with a coverslip and sealed with silicone to prevent dehydration. Microscopy images were used to determine fluorescence area (Ar, μm^2), fluorescence intensity (In, arbitrary units, AU), surface roughness, and stomatal density. For each lettuce species and incubation time, five independent microscopic fields acquired from different samples were used for quantitative image analysis, whereas the images presented in Fig. 2 are representative examples shown for illustrative purposes.

Fluorescence area and intensity (In) were determined using the ImageJ software (version 1.53k, National Institutes of Health, Bethesda, MD, USA). Five images per species and per incubation time were analyzed. Surface roughness was estimated from microscopy images using a standardized workflow implemented with the EBImage library in R (Pau et al., 2010). Briefly, the images were converted to grayscale, smoothed using a Gaussian filter to reduce noise, and then scaled by assigning the physical dimensions (197.5 μm in width and 148.1 μm in height) and the spatial resolution (0.103 μm $pixel^{-1}$). The grayscale intensity values were treated as relative surface heights. The following roughness parameters were then calculated: the arithmetic mean deviation of the surface heights, namely average roughness (Ra); the root mean square deviation of the surface heights, namely quadratic mean roughness (Rq); the difference between the maximum and minimum heights, namely maximum roughness (Rz). Stomata were visually counted in each image and then used to compute the stomatal density (Sc, N mm^{-2}).

2.5. Measurement of E. coli growth using plate counting

To measure microbial growth via colony-forming units (CFU), *E. coli* S17-1 pHC60 expressing green fluorescence was obtained from −20 °C glycerol stocks. A sterile loopful of the frozen stock was inoculated into LB broth (supplemented with 10 μg mL^{-1} tetracycline-HCl) and incubated overnight at 37 °C with aeration (220 rpm). One ml of the overnight culture was washed 3 times by centrifugation (8000 × *g* for 1 min) in physiological solution (PS, NaCl 0.85% w/v in H_2O) and finally resuspended in sterile PS. Fifty μL of the working bacterial suspension were applied to the center of the 1.5-cm-diameter leaf disks excised from the adaxial surface of RL and WL baby leaves. The bacterial working suspension was allowed to remain for 30 min to enable bacterial attachment. After attachment, the disk was sequentially washed by immersion for 30 s in three sterile Petri dishes containing 30 mL PS each, to remove non-adherent bacteria. Following washing, inoculated leaf disks were incubated at 25 °C for 5, 30, 120, 480, and 1440 min. Five disks were used for each timepoint and for each species. At each time point, individual disks were transferred into 1.5 mL microcentrifuge

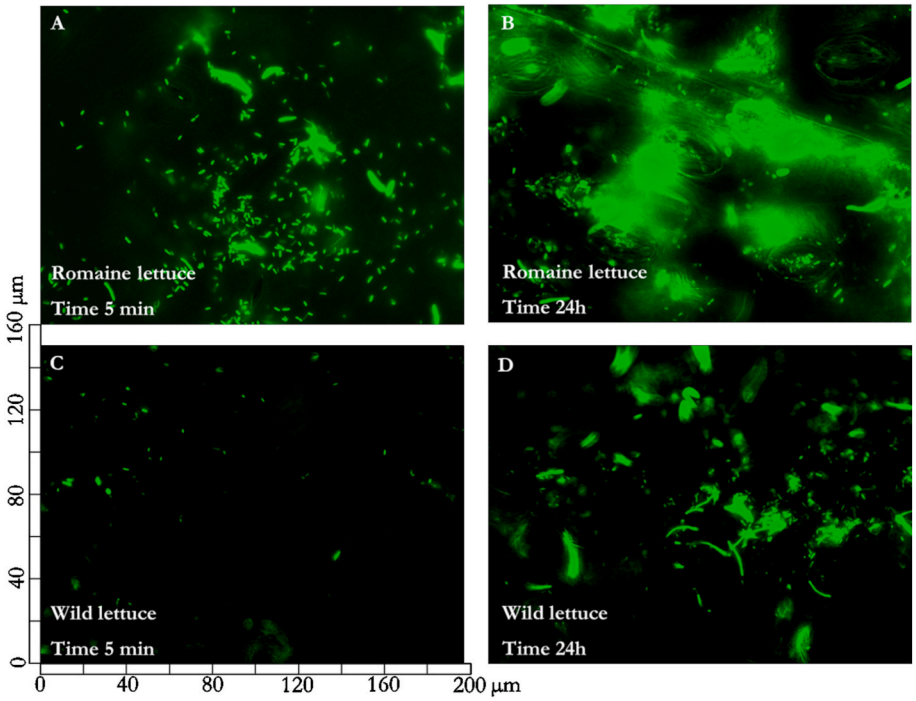

Fig. 2. Examples starting and end-point of leaf epidermis at 5 min and 24 h from the inoculation with fluorescent *E. coli*. The field size is 197.5 μm × 148.1 μm.

tubes containing 0.5 mL sterile PS and homogenized with a sterile mini-pestle. Homogenates were serially diluted, and 20 μL aliquots were spread-plated onto MacConkey agar (Oxoid, UK) supplemented with tetracycline. Plates were incubated overnight at 37 °C, and CFU were enumerated. CFU counts were transformed as log10(CFU + 1) prior to statistical analysis to accommodate samples with zero recoverable colonies.

2.6. Data and statistical analyses

The analysis of Ar and In data was performed using RStudio (R 4.3.1) (R Core Team, 2024). The normality of data was investigated using the Shapiro-Wilk's test, while homogeneity of variances was assessed using Levene's tests from the "car" package (Fox & Weisberg, 2019). Variables not exhibiting a normal distribution were transformed by using the box-cox family transformations procedure ("boxcox(.)") from the "MASS" package (Venables & Ripley, 2002). A two-way ANOVA was performed to analyse the Species (Sp) and Incubation time (It) effect on the analyzed parameters (Ar and In), and the composed parameter obtained by multiplying them (Ar×In). Five incubation times were considered: 5, 30, 120 (2 h); 480 (8 h); 1440 (24 h) minutes. Species were considered as fixed factor, while It was considered as a random effect factor. We choose a random effect on It to create a model showing the correlation between It and the analyzed parameters. Histogram or scatter-plot were used to explain the significant interactions between factors. To model the relationship between Ar and It and between Ar×In and It, second-degree polynomial equations were fitted for each species. The post-hoc analysis was performed by means of Tukey-HSD test.

The Gaussian distribution was generated using nonlinear regression to model the relationship between intensity and the average colony area for each species and incubation time. The analysis was performed in R using the "minpack.lm" library (Elzhov et al., 2016). Data were organized into a data frame, where columns represented It, Sp, replicate, intensity class (centroids of intensity intervals), and observed values. For each subset of data corresponding to specific It and Sp, the Gaussian distribution was fitted using the nonlinear least squares method (nlsLM). The following Gaussian equation was applied:

$$y = a \times \exp\left(\frac{-(x-b)^2}{2 \times c^2}\right)$$

where: y is the observed value (cumulated area), x is the intensity class, a represents the peak height, b is the center of the peak (mean intensity), c determines the spread (standard deviation) of the curve. The initial parameter estimates for the regression were a = 10, b = 55, and c = 10. Observations with negative values were excluded from the fitting process to ensure the robustness of the results. The goodness of fit for each model was evaluated using the coefficient of determination (R^2).

To model the relationship between surface roughness parameters (Ra, Rq, Rz), Sc, It, and Ar×In, we employed generalized additive models (GAMs) to account for potential nonlinear effects and interactions among predictors (Hastie & Tibshirani, 1986; Wood, 2017, 2024). Prior to model fitting, we evaluated multicollinearity among roughness descriptors using the Variance Inflation Factor (VIF) implemented in the "car" package (Fox & Weisberg, 2019). The analysis revealed severe collinearity between Ra (VIF = 20.04) and Rq (VIF = 18.94), while Rz and Sc showed acceptable VIF values (<5). To mitigate collinearity issues, Ra was excluded from the models, while Rz and Rq were retained as complementary descriptors of surface texture. The response variable was the log-transformed product of Ar×In [log(1+Ar×In)]. Predictors included It, Rq, Rz, and Sc. We fitted four GAMs: (i) a combined model including Species as a fixed effect, (ii) two species-specific models for RL and WL, and (iii) a hybrid RL + WL model based on the aggregated predictions of the species-specific GAMs.

The general structure of the combined GAM was:

$$\log(1 + Ar \times In) = \beta_0 + Species + s(Time, by = Species) + s(Rq) + s(Rz) + \beta_1 \times Sc + \varepsilon$$

Where $s(.)$ denotes smooth functions estimated using thin plate regression spline, β_0 is the intercept, β_1 represents the linear effect of Sc, and ε is the residual error term. For the species-specific models, the Species factor was excluded, and the smooth for It was fitted independently for RL and WL. All models were fitted using the restricted maximum likelihood criterion (REML) as implemented in the mgcv package (Wood, 2017).

Model validation was performed using a Monte Carlo cross-validation procedure stratified by Sp×It. In each of the 1000 iterations, five out of six replicates per stratum were randomly sampled for model training, and the remaining replicate was used for testing. Model performance was evaluated using the R^2, the Nash–Sutcliffe efficiency (NSE), the root mean squared error (RMSE), the ratio of RMSE to the standard deviation of observed data (RSR), and the percent bias (PBIAS). All analyses were conducted in R (R Core Team, 2024) using the packages "mgcv" (Wood, 2017), "dplyr" (Wickham et al., 2023), "tidyr" (Wickham & Girlich, 2023), and "car" (Fox & Weisberg, 2019) for GAM fitting, data manipulation, and collinearity assessment, respectively.

3. Results

3.1. Species and incubation are the dominant drivers (Area, intensity, and Area×Intensity)

Fluorescence imaging revealed marked differences in both fluorescence area and fluorescence intensity between RL and WL, as well as across incubation times (Fig. 2). Fig. 2 provides representative examples of bacterial colonization, whereas the reported quantitative data were obtained from replicated microscopic observations. At both 5 min and 24 h, RL (Fig. 2 A and 2 B, respectively) exhibited a larger fluorescence area than WL (Fig. 2 C and 2 D, respectively).

For both species, a progressive and significant increase in fluorescence area was observed over time (Fig. 3), with no detectable differences between 0 and 30 min, followed by a clear separation of values across longer incubation periods, following the order: 30 min <60 min h < 480 min <1440. Despite these temporal dynamics, the relative difference between RL and WL remained remarkably stable throughout the incubation period, with RL consistently exhibiting approximately twice the fluorescence area of WL. The relative increase ranged from 90% to 124% across the five sampling times, indicating that the effect of incubation time was largely independent of species. The relationship between Area and Incubation time was well described by a second-degree polynomial, with a significant R^2. The relationship between fluorescence area and Incubation time was well described by a second-degree polynomial, with a stronger fit for RL (R^2 = 0.753; y = −0.000055x2 + 0.184x + 26.751), than WL (R^2 = 0.553; y = −0.000021x2 + 0.0853x + 13.609).

These observations were further confirmed by ANOVA analyses (Supplemental Table 1). No significant interaction between Species and Incubation time was detected, while both main factors were highly significant, together accounting for up to 99.8% of the explained variability in fluorescence area. Among the two, Incubation time was the dominant driver, accounting for up to 79.6%, while Species contributed approximately 20.2%. These results highlight that temporal progression strongly shapes the observed fluorescence patterns, with species-specific effects acting consistently but independently of time.

The fluorescence Intensity displayed a less consistent temporal pattern (Fig. 4). Unlike Area, Intensity did not follow a uniform trend across incubation times, and responses differed between species. While some early and intermediate time points showed slight increases in fluorescence intensity, no clear monotonic progression was observed. The two-way ANOVA confirmed this observation (Supplemental

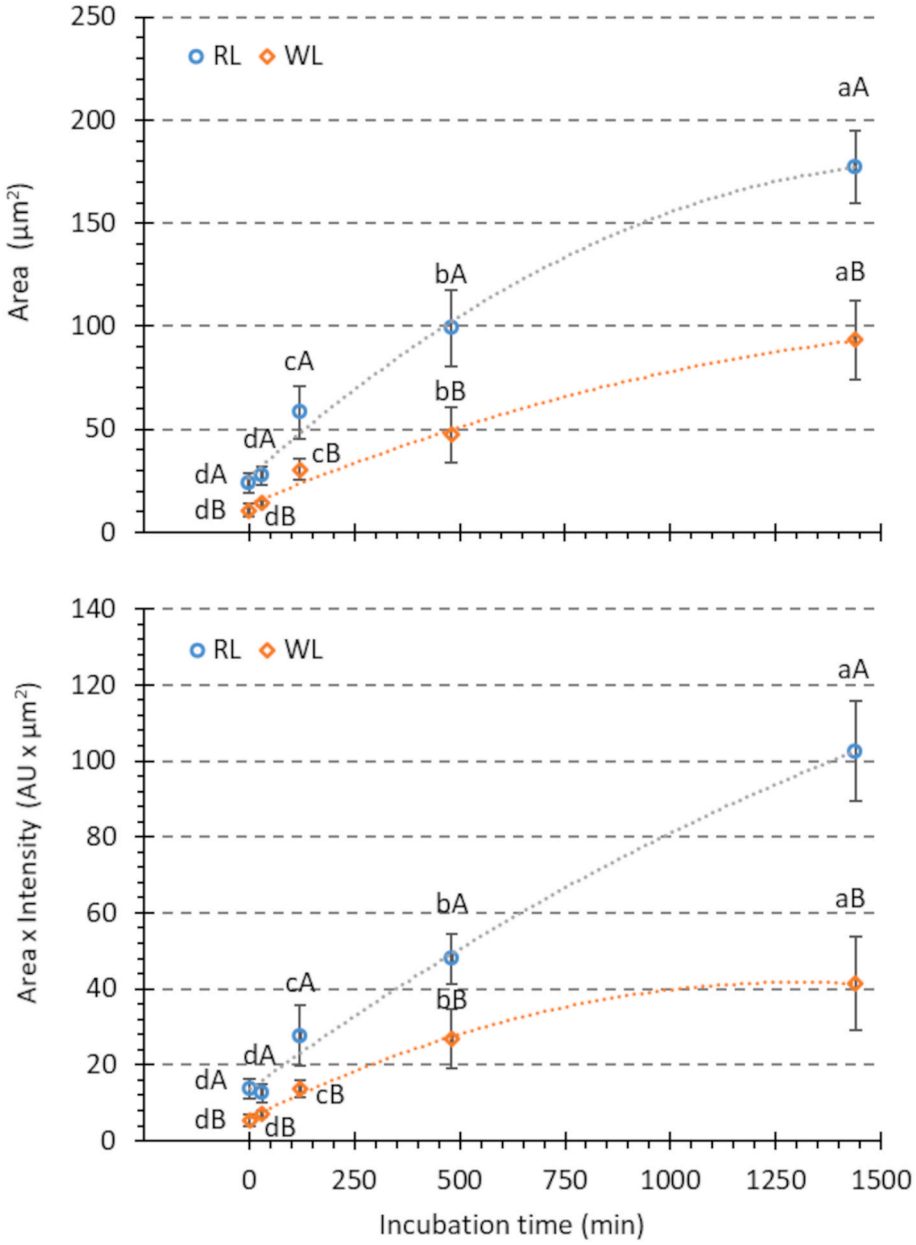

Fig. 3. Scatter plots of fluorescence Area and Area-by-Intensity over Incubation time. (A) Scatter plot showing the Fluorescence Area over Incubation Time for Romaine lettuce (RL) and wild lettuce (WL). Points represent mean values (n = 6 per time point and species), and bars indicate standard errors. Regression curves were fitted to the full dataset. Lowercase letters denote significant differences between incubation times within each species; uppercase letters denote differences between species at each time point (Tukey HSD, $p < 0.05$). Incubation times: 120 min = 2 h; 480 min = 8 h; 1440 min = 24 h. (B) Scatter plot showing Area-by-Intensity over Incubation Time for RL and WL. Points show mean values (n = 6), and bars indicate standard errors. Regression curves were fitted to the full dataset. Lettering indicates significant differences as described in (A).

Table 2), indicating a strong and significant interaction between Species and Incubation time for Intensity ($p < 0.001$), accounting for 90.4% of the explained variability. This suggests that the effect of Incubation time on Intensity differs substantially between RL and WL, unlike area, where species-specific dynamics were more stable.

When considering the composite parameter Area × Intensity, which integrates the spatial and radiometric information from fluorescence images, similar patterns were observed, though with an even stronger effect of time. Incubation time alone explained 73.8% of the variance (Supplemental Table 3), while Species contributed 23.7%, and their interaction accounted for only 2.5%, confirming that the dynamics of bacterial colonization progress similarly in both RL and WL. The polynomial models effectively described the relationship between Area × Intensity and Incubation time, with RL showing a stronger fit ($R^2 = 0.756$) than WL ($R^2 = 0.412$). This indicates a more pronounced trend in RL ($y = -0.000013x^2 + 0.080x + 13.589$), while WL follows a less defined but still significant pattern ($y = -0.000021x^2 + 0.0545x + 5.972$) (Fig. 3).

3.2. Temporal variations in colony area within intensity classes

The analysis of Fluorescence area (µm²) and the distribution of intensity classes between RL and WL revealed significant differences in growth patterns and variability over incubation time (Fig. 5; Supplemental Table 4). The average Area consistently increased for both species as incubation progressed, with RL exhibiting significantly higher

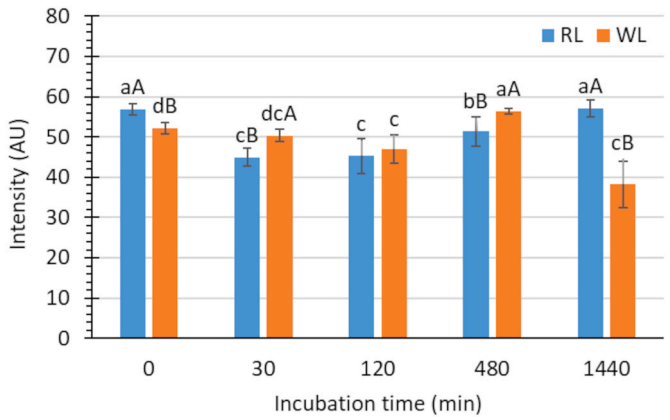

Fig. 4. Histogram plot of Intensity as function of the Incubation time for the Romaine lettuce (RL) and wild lettuce (WL). The histograms represent the average values of Intensity for the respective Incubation time. The error bars represent the standard errors. Lowercase letters indicate significant differences between Incubation times within Species, while uppercase letters indicate significant differences between Species within Incubation time according to the Tukey-HSD post-hoc test ($p < 0.05$).

values compared to WL across all Incubation times. At the initial Incubation time (5 min), RL showed an average Area of 2.4 μm^2 (SD = 3.96 μm^2), more than twice that observed in WL (1.07 μm^2; SD = 1.78 μm^2). At 1440 min, RL reached an average of 17.74 mm^2 (SD = 33.41 μm^2), almost double WL's Area (9.331 mm^2; SD = 10.35 μm^2), confirming consistently greater colony expansion in RL throughout the incubation period.

The variability of Area, expressed as standard deviation, increased over time for both species, particularly for RL, reflecting greater heterogeneity in colony sizes at later time points (Supplemental Table 4). The analysis of kurtosis and skewness highlighted differences in the shape of the distributions between species. RL showed a transition from a slightly peaked distribution (positive kurtosis) at early incubation times to a flatter distribution (negative kurtosis) at intermediate times (e.g., kurtosis = −1.095 at 480 min), followed by a return to a more peaked distribution at 1440 min (kurtosis = 1.784). WL exhibited higher kurtosis values at intermediate times, peaking at 480 min (kurtosis = 7.613), indicating a sharper concentration of values with more extreme outliers. Skewness remained consistently positive for both species, indicating right-tailed distributions, with WL showing higher skewness values overall, particularly at 480 min (skewness = 2.719), indicating a stronger asymmetry toward smaller colony areas.

The histogram analysis of the cumulative Area across intensity classes provided further insights into species-specific growth dynamics (Fig. 5). At early incubation times (5 and 30 min), both RL and WL exhibited low cumulative Area values across all intensity classes, with RL showing significantly higher WL in the lower intensity classes. As incubation progressed, RL expanded into higher intensity classes (e.g., 40–70 at 480 min and 50–80 at 1440 min), indicating the progressive development of larger and more densely colonized regions. In contrast, WL remained more concentrated within intermediate intensity classes (e.g., 30–50), suggesting a slower shift towards high-density colonization. Significant differences between species were observed in most intensity classes, particularly at later incubation times, where RL dominated the higher intensity ranges.

The Gaussian distribution analysis revealed distinct patterns for RL and WL. RL distributions were generally broader and better approximated by Gaussian fits, with higher R^2 values across all incubation times (Fig. 5). For example, at 24 h, RL had an R^2 of 0.464, compared to WL's weaker fit (R^2 = 0.209), reflecting the broader distribution of colony Area across intensity classes in RL. WL's distributions, especially at intermediate time points, were narrower and more peaked, driven by a concentration of values within intermediate intensity classes and the presence of extreme values, reflecting more clustered colony size distributions.

The temporal dynamics of the Gaussian parameters a (peak height), b (distribution spread), and c (horizontal shift) were evaluated via quadratic regression (Supplemental Table 5). For both species, parameter a showed the strongest correlation with incubation time (RL: $a = 0.000041x^2 + 0.016x + 13.075$, $R^2 = 0.999$; WL: $a = -0.000025x^2 + 0.053x + 5.318$, $R^2 = 0.99$), indicating that the relative abundance of dominant colony sizes was highly time-dependent. The spread parameter b exhibited moderate predictability in RL ($b = 0.000013x^2 - 0.013x + 51.667$, $R^2 = 0.447$) and WL ($b = -0.000011x^2 + 0.014x + 52.163$, $R^2 = 0.887$), indicating species-specific differences in distribution width over time. Finally, the horizontal shift parameter c, representing the movement of the distribution peak across intensity classes, displayed a weaker dependency on incubation time both in RL ($c = -0.000012x^2 + 0.02x + 8.624$, $R^2 = 0.672$) and WL ($c = 0.0000055x^2 - 0.006x + 8.295$, $R^2 = 0.26$). These results suggest that colony growth dynamics are primarily associated with changes in the relative abundance of dominant colony sizes (parameter a), whereas differences in distribution spread (parameter b) became more evident at intermediate and late incubation stages.

3.3. *Modeling the relationship between surface roughness, stomatal density, and fluorescence response*

The roughness and stomata data are reported in (Supplemental Table 6). No significant differences were observed for Ra and Rq parameters between the two species, while the Rz parameter and Stomatal count were found to be significantly higher in RL than in WL.

The analysis was conducted using GAMs to describe the relationship between surface roughness parameters, stomatal density, and fluorescence (Ar×In). Four model configurations were tested: (i) Combined GAM, estimating a single response function for all observations regardless of species; (ii) RL GAM and WL GAM, species-specific models that estimate independent functions for each species; (iii) RL + WL GAM, which integrates species-specific predictions by applying the RL function to RL data and the WL function to WL data.

Model performance was evaluated using Monte Carlo cross-validation stratified by incubation time (1000 iterations). The species-specific models (RL GAM and WL GAM) captured the data distribution more accurately, closely following the 1:1 line with relatively small deviations (Fig. 6). The Combined GAM exhibits greater variability and tends to underestimate higher fluorescence values, particularly for RL samples. The RL + WL GAM substantially improves prediction consistency compared to the Combined GAM, especially for high Ar×In values, by leveraging independent species-specific response functions.

The predicted proliferation curves compared with observed values over time was determined (Fig. 7). The RL GAM successfully reproduces the growth dynamics across the entire temporal range, maintaining strong alignment with the experimental data. The WL GAM accurately captures average fluorescence levels but slightly underestimates maximum responses in the later stages of incubation. In contrast, the Combined GAM shows an increasing mismatch over time, which explains its weaker overall predictive performance. The RL + WL GAM approach mitigates these discrepancies, yielding more stable predictions that are better aligned with observed dynamics.

The residuals distribution was also inferred (Fig. 8), highlighting key differences among the models: The Combined GAM shows a systematic bias, with overestimation at low fluorescence values and underestimation at high values. In the species-specific models, residuals are more symmetric and centered around zero, although RL GAM shows slightly higher variance at extreme intensity levels. The RL + WL GAM further reduces extreme errors, resulting in the best trade-off between accuracy and robustness among all evaluated models.

The GAM results are summarized in Table 1. Among the species-

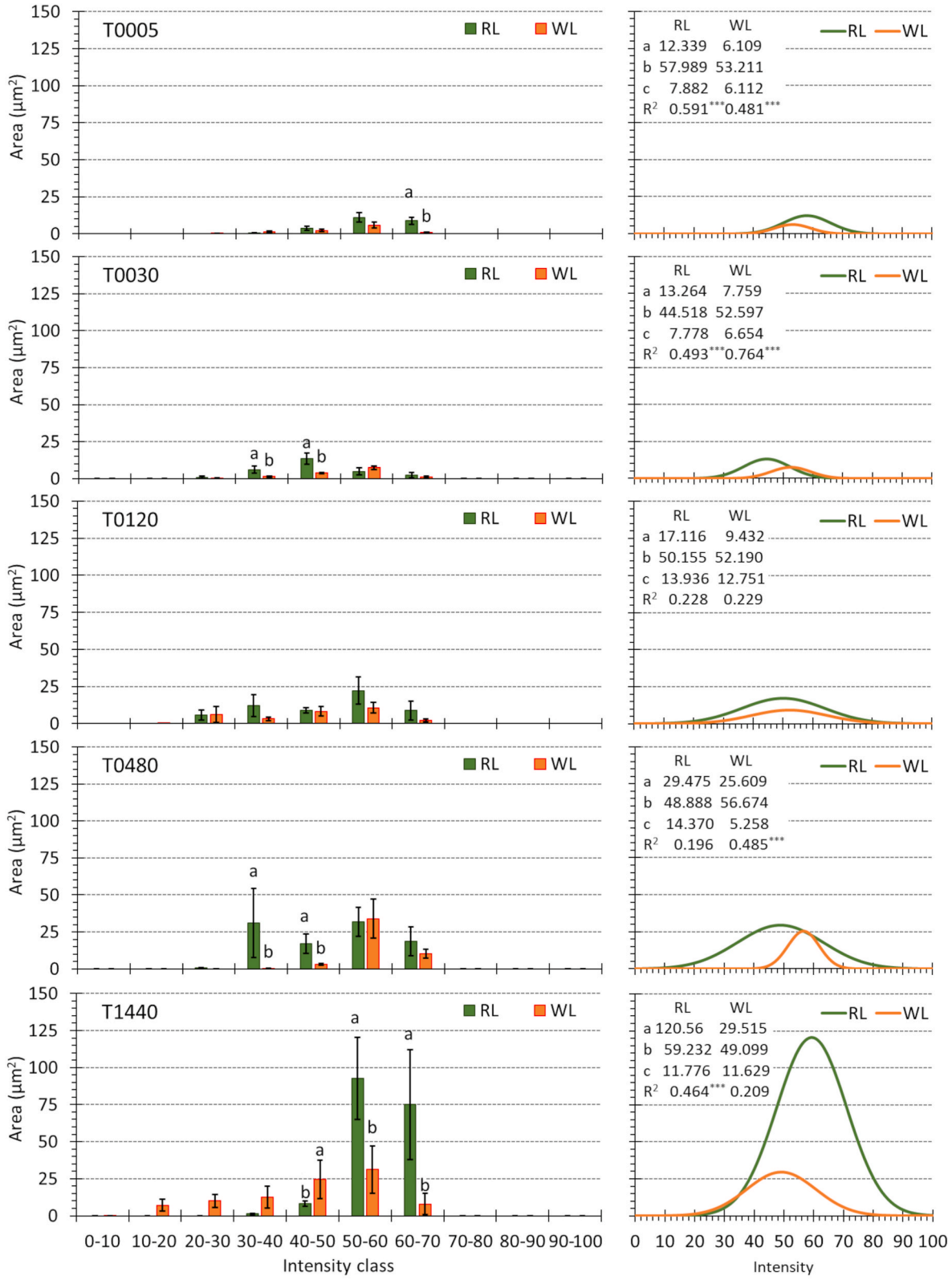

Fig. 5. Histogram plots of cumulated Area per class of Intensity for the Romaine lettuce (RL, green) and wild lettuce (WL, orange) at five Incubation times (T0005, T0030, T0120, T0480, and T1440). The bars represent the average cumulated Area for each class of Intensity, with error bars representing the standard errors. Significant differences between species within intensity classes, determined using the Tukey-HSD post-hoc test ($p < 0.05$), are denoted by different lowercase letters. The right panels display the Gaussian distribution fits for the data at each incubation time, with the corresponding coefficients (a, b, c) and R^2 for RL and WL. The curves provide an approximation of the data distribution across intensity classes for each species at each time point. (For interpretation of the references to colour in this figure legend, the reader is referred to the Web version of this article.)

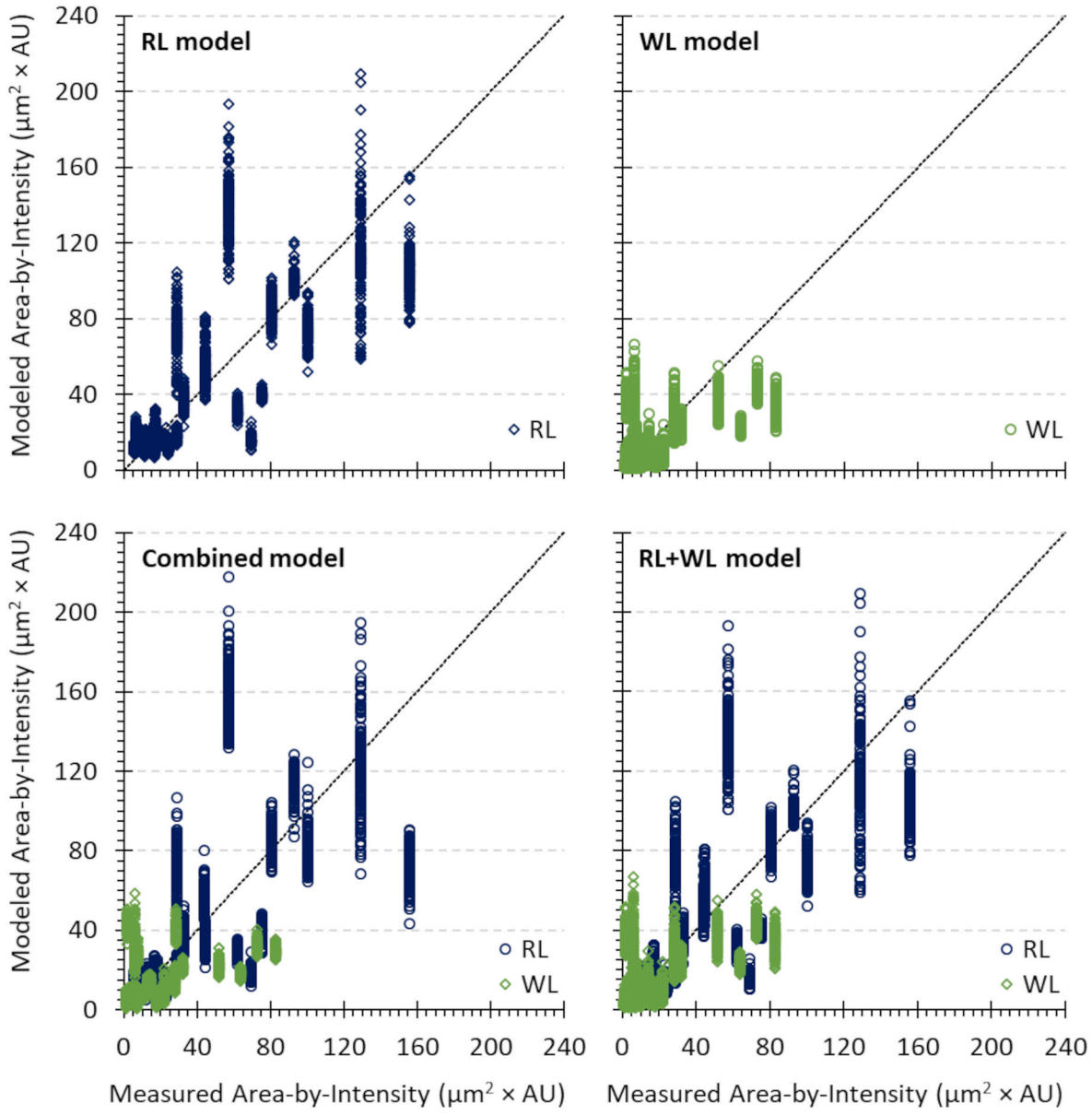

Fig. 6. Comparison between measured and generalized additive models (GAM) values for (a) RL GAM, (b) WL GAM, (c) Combined GAM, and (d) RL + WL GAM. The 1:1 dashed line represents perfect agreement between observations and predictions. Data for RL are shown in blue, while data for WL are shown in green. (For interpretation of the references to colour in this figure legend, the reader is referred to the Web version of this article.)

specific models, the RL GAM achieved the best overall performance, explaining nearly 78% of the deviance and providing the most accurate and stable predictions, with the lowest systematic bias. The WL GAM explained approximately 61% of the deviance and, although it yielded lower average prediction errors, showed a greater tendency to overestimate fluorescence values. The Combined GAM, which relied on a single response function for both species, exhibited the weakest overall performance, explaining about 67% of the deviance and showing the highest residual dispersion, indicating that a common response function was unable to fully capture species-specific colonization dynamics. By contrast, the RL + WL GAM, which combines independent species-specific functions, provided the best compromise between accuracy and generalizability. Although its explanatory power was lower than that of the RL GAM alone, it reduced prediction errors relative to the Combined GAM while maintaining robust predictive performance across the full range of fluorescence values. These results indicate that incorporating species-specific response functions substantially improves model performance, particularly for the intermediate and high fluorescence ranges where RL and WL exhibit distinct colonization patterns.

Analysis of the contribution of individual predictors highlighted consistent patterns across models (Table 2). For RL GAM, incubation time dominated the response, accounting for over 90% of the explained variance, while surface roughness metrics played a minor role. WL GAM showed a similar structure but with a lower contribution of incubation time (≈62%) and a stronger influence of maximum roughness (≈32%). In the Combined GAM, incubation time remained the main driver, but its effect differed markedly between species: approximately 52% for RL and 29% for WL, confirming the distinct temporal dynamics. The RL + WL GAM successfully captures these differences, with incubation time explaining nearly 77% of the variance, complemented by the contribution of maximum roughness (≈20%).

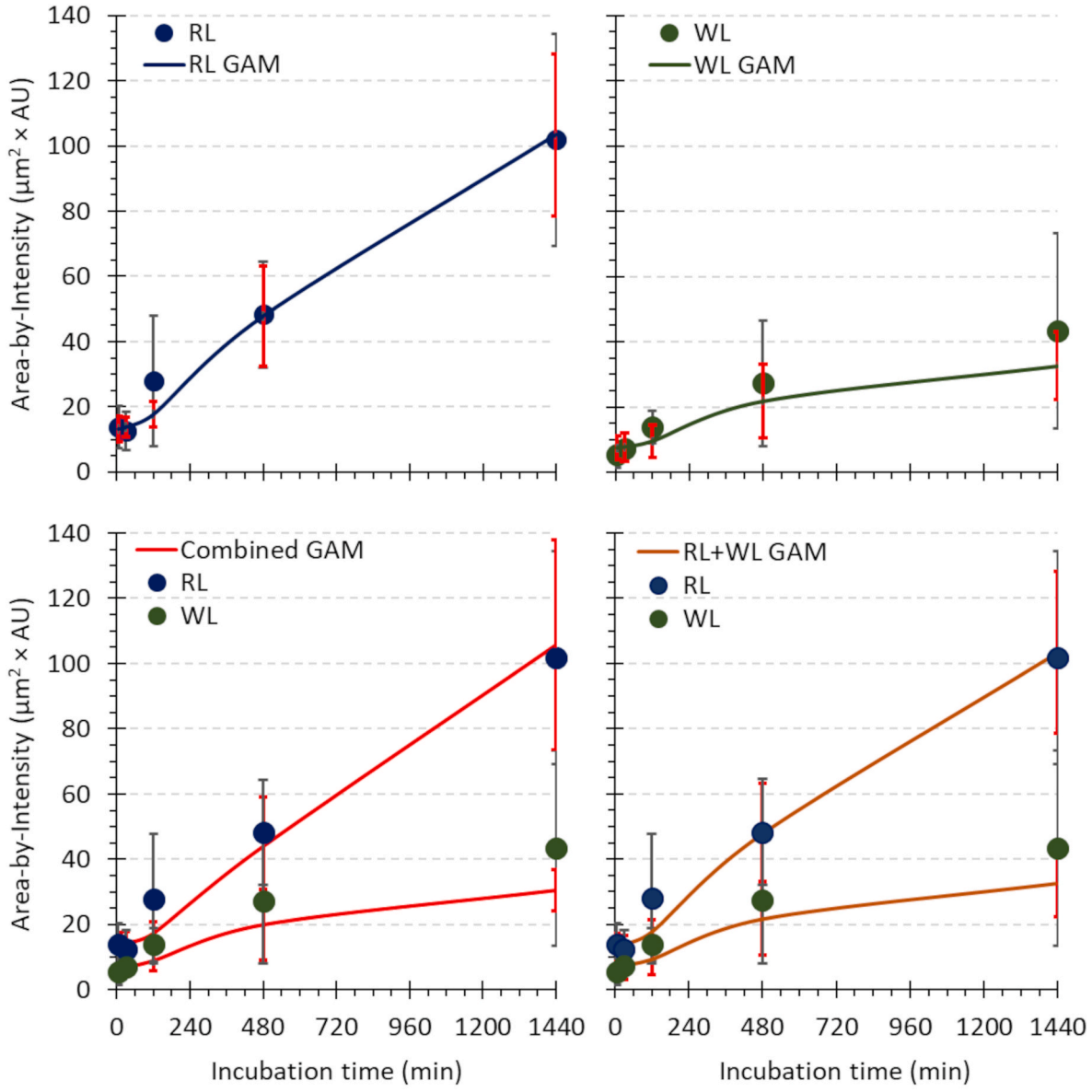

Fig. 7. Panels show the predicted fluorescence proliferation dynamics (Ar·In) over incubation time for the four generalized additive models (GAM) configurations.: (top-left) RL GAM, (top-right) WL GAM, (bottom-left) Combined GAM, and (bottom-right) RL + WL GAM. Observed data are shown as points (blue for RL and green for WL), with grey error bars representing the standard deviation of the measured values. Solid lines represent model predictions, with red error bars indicating the uncertainty of the predicted means. (For interpretation of the references to colour in this figure legend, the reader is referred to the Web version of this article.)

3.4. Analysis of microbial growth using plate counting on WL and RL surfaces over time

E. coli proliferation on leaf surfaces quantified over time by plate counting (log CFU disc^{-1}) revealed significant differences between WL and RL at 30 min ($p < 0.05$), 480 min ($p < 0.01$), and 1440 min ($p < 0.001$) (Supplemental Table 7). For WL, bacterial proliferation remained low and relatively stable during the early phases (5 to 480 min), with values ranging between 0.82 ± 0.78 and 1.09 ± 0.86 log CFU disc^{-1}. A significant increase was observed only at 1440 min ($p < 0.05$). In contrast, RL showed a continuous and more pronounced increase in bacterial counts throughout the incubation period. Starting from 1.37 ± 1.02 log CFU disc^{-1} at 5 min, RL values rose steadily, peaking at 3.22 ± 3.12 log CFU disc^{-1} at 1440 min. The largest increase occurred between 120 min and 480 min, where a statistically significant jump was detected ($p < 0.05$). Overall, plate counting indicated consistently higher bacterial counts on RL than on WL, particularly after 480 min, when proliferation on RL markedly exceeded that observed on WL.

4. Discussion

In this study, we monitored the growth of an *E. coli* strain expressing GFP on the surface of lettuce baby leaves using an integrated approach that combines high-resolution fluorescence microscopy with predictive modeling based on Generalized Additive Models (GAMs). Our results demonstrate the potential of this framework as the basis for predictive monitoring approaches, complementing standard plating-based measurements and supporting the development of predictive relationships between leaf surface traits and bacterial proliferation patterns.

Green Fluorescent Protein has been widely applied to monitor bacterial infections in living plants at cellular and whole-plant scales (Wang et al., 2007). In the present study, GFP-labelled bacteria were used as experimental tracers to enable high-resolution visualization of colonization dynamics under controlled conditions rather than as a direct detection strategy applicable to post-harvest processing environments.

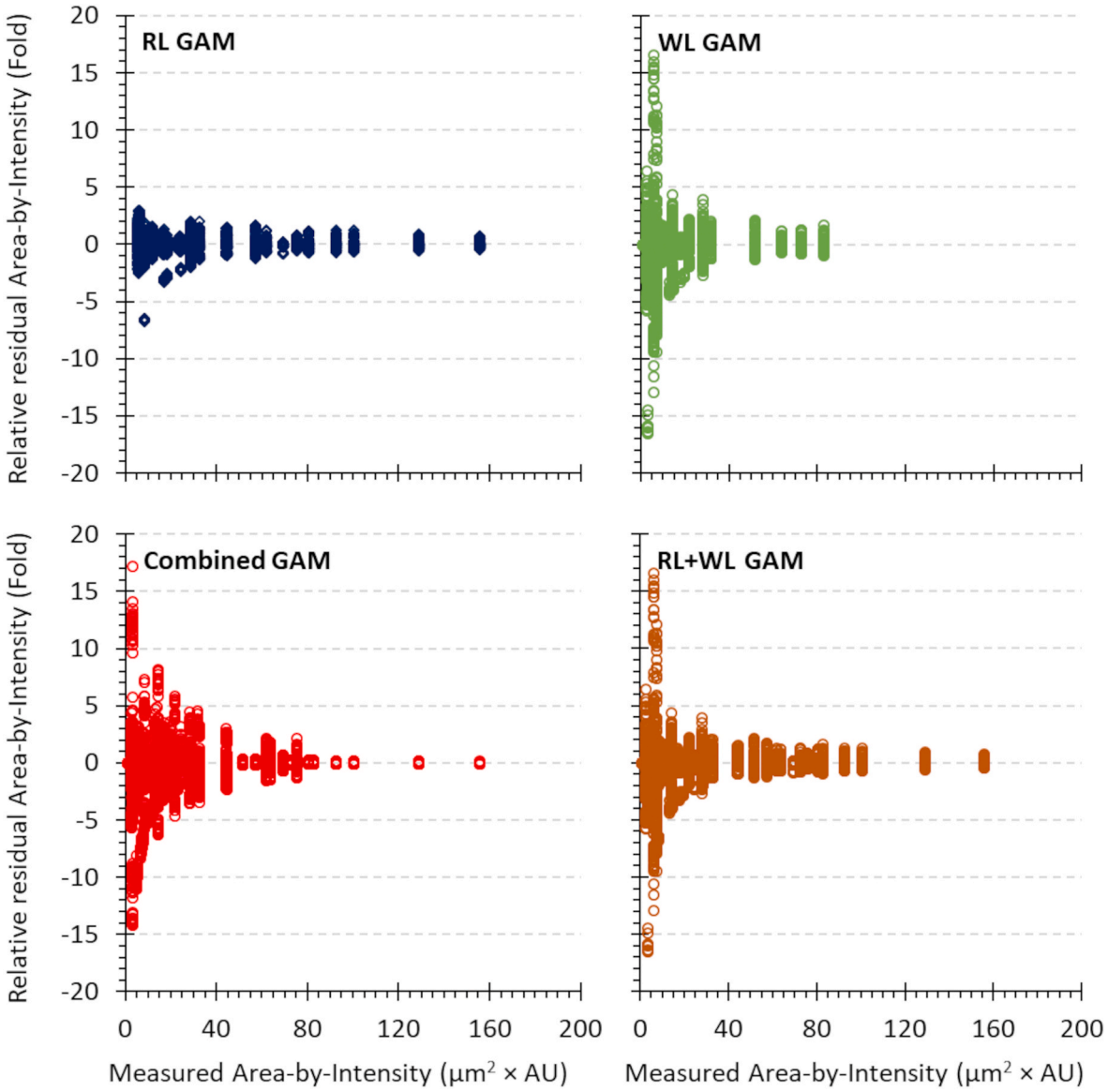

Fig. 8. Residual distribution of the four generalized additive models (GAM) configurations for predicting fluorescence (Ar·In). Each panel shows residuals (predicted minus measured values) plotted against the measured fluorescence for the RL GAM (top-left, blue), WL GAM (top-right, green), Combined GAM (bottom-left, red), and RL + WL GAM (bottom-right, brown). (For interpretation of the references to colour in this figure legend, the reader is referred to the Web version of this article.)

Table 1
Performance comparison of the four generalized additive models (GAM) configurations for predicting fluorescence (Ar·In). The table reports the main accuracy and error metrics: coefficient of determination (R^2), Nash–Sutcliffe efficiency (NSE), root mean square error (RMSE, μm^2·AU), ratio of standard deviation of residuals to observations (RSR), and percentage bias (PBIAS, %).

Model	R^2	Mean explained deviance (%)	NSE	RMSE (μm^2 * AU)	RSR	PBIAS (%)
Combined GAM	0.471	0.675	0.394	25.52	0.78	11.18
RL GAM	0.584	0.777	0.539	25.89	0.68	4.18
WL GAM	0.413	0.607	0.381	16.98	0.79	18.84
RL + WL GAM	0.584	0.692	0.554	21.89	0.67	8.9

Positive PBIAS values indicate model overestimation, whereas negative values indicate model underestimation.

Table 2
Percentage of variance explained by each predictor across GAM configurations. Values are reported as mean (standard deviation) over 1000 Monte Carlo iterations.

Predictor	Percentage of variance explained			
	Combined GAM	RL GAM	WL GAM	RL + WL GAM
Incubation_time: RL	52.5 (6.65)			
Incubation_time: WL	28.9 (6.35)			
Incubation_time		91.6 (3.61)	62.3 (12)	77 (7.81)
Rz	12.5 (5.9)	7.2 (3.36)	32.2 (11.5)	19.7 (7.43)
Rq	6.1 (2.86)	1.2 (1.33)	5.5 (4.78)	3.3 (3.06)

While previous studies have shown GFP intensity to be a reliable proxy for bacterial quantification in suspension and biofilm settings (Wilson et al., 2018), our results indicate that in the context of leaf surfaces, intensity does not consistently correlate with bacterial (micro-)colony area, limiting its use as a stand-alone quantification metric. Further

development of this approach, possibly coupled with confocal laser scanning microscope, could involve combining endogenous GFP expression with propidium iodide (PI) staining to enable simultaneous assessment of bacterial viability and growth at single-cell resolution under physiologically relevant conditions (Avalos Vizcarra et al., 2013). The experimental system adopted in this study was specifically designed to overcome the optical limitations associated with quantitative fluorescence imaging of intact lettuce leaves at single-cell resolution. Although previous studies have successfully visualized GFP-labelled bacteria within intact leaf tissues, these investigations primarily focused on localized observations of bacterial attachment or internalization rather than repeated quantitative monitoring of early micro-colony development (Chahar et al., 2021; Kroupitski, Golberg, et al., 2009; Zhou et al., 2018). By combining isolated epidermal layers with species-specific plant juice–agar media, we established a reproducible imaging platform that preserved the leaf surface architecture relevant for bacterial attachment while providing host-derived nutrients and enabling continuous quantitative measurements of bacterial colonization under controlled experimental conditions.

Two fluorescence-based parameters were analyzed: (i) fluorescence area (μm^2), representing the spatial extent of colonization, and (ii) fluorescence intensity (a.u.), reflecting the local signal density and potentially the concentration of aggregated bacteria. While the fluorescence area showed a consistent and significant increase over time, fluorescence intensity displayed a more complex dynamic, with a mild initial increase followed by stabilization and, in some cases, slight decreases at later stages. Similar behavior has been reported in fluorescence-based studies of bacterial colonization, where signal intensity may vary independently from cell abundance due to structural heterogeneity within developing microcolonies and biofilms (Brandl, 2009; Kroupitski, Pinto, et al., 2009). This suggests that fluorescence intensity alone may not reliably track bacterial proliferation on leaf surfaces, likely due to heterogeneous biofilm development and structure, metabolic adaptations, or changes in GFP expression during stationary phases (Deering et al., 2012; Seo & Frank, 1999). Consequently, combining area and intensity (Ar×In) provides a more robust measure of colonization dynamics and was therefore adopted for predictive modeling purposes. Similar composite fluorescence metrics have been successfully applied to describe spatial organization and growth dynamics of bacterial populations on plant tissues and abiotic surfaces (Dublan et al., 2014; Remus-Emsermann & Schlechter, 2018). This combined metric therefore, represents a robust proxy for describing micro-colony development under controlled experimental conditions.

Several studies have highlighted differing levels of susceptibility to human pathogen contamination across various types of vegetables (Hunter et al., 2015; Jacob & Melotto, 2020; Lenzi et al., 2022; Truschi et al., 2023). In our study, romaine lettuce (RL) consistently exhibited larger colonization areas and higher cumulative fluorescence levels than wild lettuce (WL) at all incubation times, confirming a significantly greater susceptibility to bacterial proliferation. Interestingly, substantial differences in fluorescence coverage were already observed at the earliest sampling time (5 min post-inoculation). Because bacterial proliferation is expected to be negligible over such a short incubation period, these differences are more likely to reflect the initial attachment and spatial retention of bacterial cells than active cell division. Such early attachment events are strongly influenced by leaf surface characteristics, including epicuticular wax composition, surface hydrophobicity, roughness, and stomatal density (Truschi et al., 2023, 2024). Notably, the RL cultivar "Bionda degli Ortolani," previously identified as among the most susceptible baby-leaf varieties within a panel of 30 accessions (Truschi et al., 2023), displayed extensive colonization in the present study, underscoring the importance of cultivar-level variability in microbial risk assessment. These findings are consistent with previous studies (Jacob & Melotto, 2020; Truschi et al., 2023), which reported a reduced colonization capacity in wild lettuce genotypes, likely driven by differences in leaf surface architecture. In a recent investigation, Truschi et al. (2024) demonstrated that surface hydrophobicity, largely modulated by epicuticular wax composition, and particularly by the presence of three-dimensional wax crystals of C26 alcohol, plays a central role in limiting bacterial adhesion. Wild lettuce, characterized by a higher degree of hydrophobicity and a distinct waxy profile (Truschi et al., 2024), exhibited significantly lower adhesion of *Salmonella enterica* compared to romaine lettuce, supporting the hypothesis that surface physiology strongly influences pathogen attachment. Therefore, the differences observed immediately after inoculation most likely reflect species-specific retention processes that establish the initial conditions for subsequent bacterial proliferation, rather than differences in bacterial growth rates.

Surface micro-morphology played a central role in colonization patterns. Among the roughness parameters, the maximum vertical surface variation (Rz), emerged as a key determinant of bacterial proliferation, explaining up to 19–32% of variance in predictive models. Similarly, stomatal density was significantly higher in RL and, together with Rz, likely increased the availability of micro-niches for bacterial retention and protection. These findings align with previous reports linking surface topography to enhanced bacterial adhesion and biofilm formation (Kroupitski, Pinto, et al., 2009; Macarisin et al., 2013; Palma-Salgado et al., 2020) and explain why RL surfaces, characterized by more complex microstructures, and thus, higher surface area, supported higher proliferation levels than WL. Such structural variability between cultivars highlights the importance of considering leaf morphology in microbiological risk assessment and supports the need for predictive tools capable of accounting for species- or cultivar-specific behavior.

To better understand colonization dynamics, we applied Generalized Additive Models (GAMs) to integrate incubation time, morphological traits, and fluorescence responses. Unlike mechanistic microbial growth models, the proposed GAM framework is not intended to estimate intrinsic bacterial growth parameters. Rather, it quantifies the relative contribution of temporal and leaf surface characteristics to the observed colonization dynamics. Species-specific GAMs provided the highest predictive accuracy, with the RL model explaining up to 91% of the observed variance and the WL model capturing the main fluorescence trends despite slightly higher variability and a modest positive bias. The RL + WL GAM, which combined independent species-specific functions, achieved a robust compromise between accuracy and generalizability: compared with the Combined GAM, it reduced average prediction errors by approximately 15% and improved predictions across intermediate and high fluorescence ranges. By contrast, the Combined GAM, based on a single response function, showed weaker performance, underestimating high fluorescence values and failing to capture species-specific colonization dynamics. These models therefore represent the main transferable outcome of the study, as they provide a quantitative framework linking leaf surface traits to colonization dynamics independently of the specific fluorescence detection strategy adopted, consistent with recent efforts to integrate structural leaf traits into predictive microbial models for fresh produce systems (Mishra et al., 2017; Sant'Ana et al., 2012).

Across all model configurations, incubation time was consistently proven as the most influential predictor, confirming its central role in bacterial colonization kinetics on leaf surfaces, as widely reported for epiphytic growth of enteric pathogens on leafy vegetables (Brandl, 2006; Erickson, 2012). However, morphological traits, particularly maximum roughness (Rz), also contributed substantially to model performance, highlighting their relevance in predicting colonization risk. By contrast, Rq (mean roughness) had only a minor effect, and stomatal density contributed indirectly, likely through its interaction with surface microtopography. These findings support previous observations that microscale leaf surface structure influences bacterial attachment, retention, and aggregation patterns in the phyllosphere (Barak et al., 2013; Kroupitski, Pinto, et al., 2009; Remus-Emsermann & Schlechter, 2018). Together, these results indicate that while time remains the

dominant driver of microbial proliferation, micro-morphological features act as important modifiers of colonization patterns and should therefore be considered in risk-oriented predictive frameworks.

By integrating fluorescence-based measurements with predictive GAMs, this study establishes a quantitative framework linking leaf surface microtopology to early bacterial micro-colony development, improving our understanding of how bacterial populations organize and expand on leaf surfaces under controlled experimental conditions.

Fluorescence-based quantification was also compared with traditional colony-forming unit (CFU) counts. While CFU plating remains the standard method for enumerating viable culturable cells, fluorescence microscopy enabled visualization of the early spatial organization and development of bacterial micro-colonies before substantial changes became apparent in plate counts. Because fluorescence-derived descriptors and CFU enumeration quantify different aspects of bacterial colonization, the two approaches should be regarded as complementary rather than directly comparable. Conventional CFU enumeration requires homogenization of the leaf tissue before plating, providing an estimate of the total number of recoverable culturable cells but inevitably disrupting the spatial organization of bacterial populations on the leaf surface. Consequently, CFU measurements cannot capture the initial attachment, aggregation, and spatial organization of bacterial cells into developing micro-colonies, phenomena that characterize the early stages of bacterial colonization on leafy vegetables (Deering et al., 2012; Seo & Frank, 1999). This limitation is particularly relevant during the early phases of colonization, when bacterial cells are heterogeneously distributed across the leaf surface and their behavior is influenced by microscale interactions and stochastic processes (Manios et al., 2013). Although the use of GFP-labelled bacteria is not directly transferable to industrial monitoring applications, fluorescence imaging provides a valuable experimental platform for investigating early colonization dynamics under controlled conditions and for establishing predictive relationships between leaf surface characteristics and bacterial proliferation.

The objective of the proposed GAM framework is not to replace conventional predictive microbiology models but to complement them by incorporating microscale structural descriptors of the leaf surface that are generally not considered in traditional growth models. A number of studies have described bacterial growth on leafy vegetables using classical predictive models based on changes in microbial populations over time (Mishra et al., 2017; Sant'Ana et al., 2012). Other modeling approaches are related to the Quantitative Microbial Risk Assessment model (QMRA), likelihood of illness from exposure to pathogens in food, water, or the environment (Bulut et al., 2025; Pang et al., 2017). However, to our knowledge this study represents one of the first attempts to model the early development of bacterial micro-colonies directly at the leaf surface starting from single-cell observations. Future developments may include high-throughput fluorescence imaging approaches combined with GAM-based prediction to support quantitative assessment of colonization risk and pathogen growth on leafy vegetables. In this context, fluorescence imaging should therefore be interpreted primarily as a calibration platform for model development rather than as a direct industrial detection technology. Given the repeated implication of romaine lettuce in large-scale *E. coli* O157:H7 outbreaks (Coulombe et al., 2020; Slayton et al., 2013; Waltenburg et al., 2022), the adoption of predictive, real-time monitoring tools has the potential to enhance microbial safety and improve traceability in the fresh-cut produce industry.

Despite providing promising insights into fluorescence-based monitoring of bacterial proliferation, this study has several limitations that should be considered when interpreting the results. First, the experiments were performed under controlled laboratory conditions and at a single incubation temperature (37 °C), corresponding to the optimal growth temperature of *E. coli*. Consequently, the colonization dynamics observed over time are specific to these experimental conditions and should not be directly extrapolated to industrial environments, where temperature, humidity, and processing-related stresses vary substantially. Future studies should therefore validate the proposed predictive framework under commercially relevant conditions, particularly across the temperature ranges encountered during the fresh-cut produce cold chain. Second, fluorescence observations were performed on isolated adaxial epidermal layers placed on species-specific plant juice–agar media to overcome the optical limitations associated with quantitative fluorescence imaging of intact lettuce leaves. This experimental configuration preserves the principal leaf surface micro-morphological traits involved in bacterial attachment while enabling reproducible high-resolution imaging. However, it does not fully reproduce the three-dimensional architecture and physiological complexity of intact leaves, including tissue organization, water dynamics, and plant responses that may influence bacterial colonization. Therefore, the proposed system should be regarded as a controlled, biologically informed platform for quantitatively investigating early colonization dynamics rather than as a direct representation of post-harvest contamination processes. Third, although fluorescence microscopy allowed us to track bacterial colonization with high spatial resolution, fluorescence intensity alone showed inconsistent correlation with bacterial abundance, particularly at later incubation stages, likely due to metabolic shifts or altered GFP expression. This highlights the need to validate fluorescence-derived metrics against absolute bacterial counts under a wider range of physiological conditions. Furthermore, the study focused on a single, non-pathogenic bacterial strain (*E. coli* expressing GFP) and two lettuce genotypes, which limits the generalizability of the findings. Different pathogen species and host genotypes are known to exhibit distinct attachment strategies and colonization behaviors on leaf surfaces, and these aspects should be systematically explored in future studies. Additionally, while our Generalized Additive Models (GAMs) demonstrated strong predictive performance, model robustness was evaluated using Monte Carlo simulations based on a limited dataset; further validation with larger, independent datasets and under real-world processing conditions will be required before implementation in industrial monitoring systems. Finally, although we demonstrate the feasibility of integrating high-resolution imaging with predictive modeling, the scalability of fluorescence microscopy for in-line high-throughput applications remains a challenge, especially in terms of acquisition speed, cost, and automation. Future developments should explore optimized imaging systems, advanced machine learning algorithms, and multispectral detection platforms to overcome these constraints and enable robust, real-time monitoring in fresh-cut salad production chains.

Finally, although this study demonstrates the feasibility of integrating high-resolution imaging with predictive modeling, the scalability of fluorescence microscopy for in-line high-throughput applications remains a major challenge, particularly in terms of acquisition speed, cost, and automation. Future developments should therefore focus on translating the relationships identified here into alternative sensing strategies compatible with industrial environments, including optimized imaging systems, machine-learning-based image analysis pipelines, and multispectral detection platforms capable of supporting robust, real-time monitoring in fresh-cut salad production chains.

5. Conclusions

This study shows that combining high-resolution fluorescence imaging with Generalized Additive Models offers a robust framework for describing early bacterial colonization dynamics on lettuce leaf surfaces under controlled experimental conditions. The use of GFP-labelled *Escherichia coli* made it possible to visualize micro-colony development in detail and to identify the main factors driving proliferation. Incubation time emerged as the strongest predictor, while leaf surface micro-morphological traits, particularly maximum roughness (Rz), also contributed meaningfully to model performance.

Although fluorescence imaging based on genetically labelled bacteria cannot be directly applied to post-harvest monitoring systems, it

provides an effective calibration platform for establishing predictive relationships between leaf surface structure and microbial growth. Within this framework, the GAM-based models represent the most transferable outcome of the study, as they enable a quantitative assessment of how temporal and morphological factors jointly influence bacterial proliferation, independently of the specific fluorescence detection strategy used.

Overall, this integrated approach advances our understanding of bacteria–leaf surface interactions and supports the development of predictive tools for evaluating cultivar-dependent susceptibility to contamination (with pathogenic strains), with potential implications for future risk-assessment strategies in fresh-cut salad production systems.

CRediT authorship contribution statement

Stefania Truschi: Conceptualization, Data curation, Investigation, Methodology, Visualization, Writing – original draft. **Marianna Arvaniti:** Conceptualization, Investigation, Methodology, Resources, Writing – original draft. **Marco Napoli:** Formal analysis, Investigation, Methodology, Validation, Visualization, Writing – original draft, Writing – review & editing. **Massimiliano Marvasi:** Conceptualization, Funding acquisition, Investigation, Methodology. **Anna Lenzi:** Conceptualization, Funding acquisition, Project administration, Resources, Supervision, Writing – review & editing. **Panagiotis Skandamis:** Conceptualization, Funding acquisition, Methodology, Project administration, Resources, Supervision, Writing – review & editing.

Declaration of competing interest

The authors declare that they have no known competing financial interests or personal relationships that could have appeared to influence the work reported in this paper.

Acknowledgments

Project funded under the National Recovery and Resilience Plan (NRRP), Mission 4 Component 2 Investment 1.4 - Call for tender No. 3138 of 16 December 2021, rectified by Decree n.3175 of 18 December 2021 of Italian Ministry of University and Research funded by the European Union – NextGenerationEU. Award Number: Project code CN_00000033, Concession Decree No. 1034 of 17 June 2022 adopted by the Italian Ministry of University and Research, CUP B83C22002910001, Project title “National Biodiversity Future Center - NBFC”.

We thank Marianna Gregorio for some of the technical assistance.

Appendix A. Supplementary data

Supplementary data to this article can be found online at https://doi.org/10.1016/j.foodcont.2026.112448.

Data availability

Data will be made available on request.

References

Arvaniti, M., Balomenos, A., Papadopoulou, V., Tsakanikas, P., & Skandamis, P. (2024). Modelling the colony growth dynamics of Listeria monocytogenes single cells after exposure to peracetic acid and acidic conditions. *Food Research International, 191*, Article 114684. https://doi.org/10.1016/J.FOODRES.2024.114684

Avalos Vizcarra, I., Emge, P., Miermeister, P., Chabria, M., Konradi, R., Vogel, V., & Möller, J. (2013). Fluorescence-based in situ assay to probe the viability and growth kinetics of surface-adhering and suspended recombinant bacteria. *Biointerphases, 8* (1), 22. https://doi.org/10.1186/1559-4106-8-22

Banach, J. L., Sampers, I., Van Haute, S., & der Fels-Klerx, H. J. (2015). Effect of disinfectants on preventing the cross-contamination of pathogens in fresh produce washing water. *International Journal of Environmental Research and Public Health, 12*, 8658–8677. https://doi.org/10.3390/ijerph120808658

Barak, S., Mudgil, D., & Khatkar, B. S. (2013). Relationship of gliadin and glutenin proteins with dough rheology, flour pasting and bread making performance of wheat varieties. *LWT - Food Science and Technology, 51*(1), 211–217. https://doi.org/10.1016/j.lwt.2012.09.011

Beuchat, L. R. (2002). Ecological factors influencing survival and growth of human pathogens on raw fruits and vegetables. *Microbes and Infection, 4*, 413–423. https://doi.org/10.1016/S1286-4579(02)01555-1

Brandl, M. T. (2006). Fitness of human enteric pathogens on plants and implications for food safety. *Annual Review of Phytopathology, 44*, 367–392. https://doi.org/10.1146/ANNUREV.PHYTO.44.070505.143359/CITE/REFWORKS. Volume 44, 2006.

Brandl, M. T. (2009). Applying fluorescence microscopy to the investigation of the behavior of foodborne pathogens on produce. *Scanning, 2009*, 376–380. https://doi.org/10.1117/12.821816

Bulut, E., Murphy, S. I., Strawn, L. K., Danyluk, M. D., Wiedmann, M., & Ivanek, R. (2025). Risk assessment of Escherichia coli O157:H7 along the farm-to-fork fresh-cut romaine lettuce supply chain. *Scientific Reports, 15*(1), Article 17421. https://doi.org/10.1038/s41598-025-01585-z

Centers for Disease Control, & Prevention. (2022). In *E. coli O157:H7* (pp. 12–21). https://www.cdc.gov/ecoli/2021/o157h7-12-21/index.html.

Chahar, M., Kroupitski, Y., Gollop, R., Belausov, E., Melotto, M., & Sela-Saldinger, S. (2021). Determination of Salmonella enterica leaf internalization varies substantially according to the method and conditions used to assess bacterial localization. *Frontiers in Microbiology, 12*, Article 622068. https://doi.org/10.3389/FMICB.2021.622068/TEXT

Cheng, H. P., & Walker, G. C. (1998). Succinoglycan is required for initiation and elongation of infection threads during nodulation of alfalfa by Rhizobium meliloti. *Journal of Bacteriology, 180*(19), 5183–5191. https://doi.org/10.1128/JB.180.19.5183-5191.1998. WEBSITE:WEBSITE:ASMJ;ISSUE:ISSUE:DOI.

Coulombe, G., Catford, A., Martinez-Perez, A., & Buenaventura, E. (2020). Outbreaks of Escherichia coli O157:H7 infections linked to romaine lettuce in Canada from 2008 to 2018: An analysis of food safety context. *Journal of Food Protection, 83*, 1444–1462. https://doi.org/10.4315/JFP-20-029

Deering, A. J., Mauer, L. J., & Pruitt, R. E. (2012). Internalization of E. coli O157:H7 and Salmonella spp. in plants: A review. *Food Research International, 45*(2), 567–575. https://doi.org/10.1016/J.FOODRES.2011.06.058

Delaquis, P., Bach, S., & Dinu, L. D. (2007). Behavior of Escherichia coli O157:H7 in leafy vegetables. *Journal of Food Protection, 70*, 1966–1974. https://doi.org/10.4315/0362-028X-70.8.1966

Donaldson, L. (2020). Autofluorescence in plants. *Molecules, 25*(10), 2393. https://doi.org/10.3390/MOLECULES25102393, 2020, Vol. 25, Page 2393.

Dublan, M. D. L. A., Ortiz-Marquez, J. C. F., Lett, L., & Curatti, L. (2014). Plant-Adapted Escherichia coli show increased lettuce colonizing ability, resistance to oxidative stress and chemotactic response. *PLoS One, 9*(10), Article e110416. https://doi.org/10.1371/JOURNAL.PONE.0110416

Elzhov, T. V., Mullen, K. M., Spiess, A.-N., & Bolker, B. (2016). Minpack.lm: R interface to the Levenberg-marquardt nonlinear least-squares algorithm found in MINPACK, plus support for bounds. https://cran.r-project.org/package=minpack.lm.

Erickson, M. C. (2012). Internalization of fresh produce by foodborne pathogens. *Annual Review of Food Science and Technology, 3*(1), 283–310. https://doi.org/10.1146/ANNUREV-FOOD-022811-101211/CITE/REFWORKS

Fox, J., & Weisberg, S. (2019). *An R companion to applied regression* (3rd ed.). SAGE Publications, Inc.

Hastie, T., & Tibshirani, R. (1986). Generalized additive models. *Statistical Science, 1*(3), 297–318.

Hunter, P. J., Shaw, R. K., Berger, C. N., Frankel, G., Pink, D., & Hand, P. (2015). Older leaves of lettuce (Lactuca spp.) support higher levels of Salmonella enterica ser. Senftenberg attachment and show greater variation between plant accessions than do younger leaves. *FEMS Microbiology Letters, 362*. https://doi.org/10.1093/femsle/fnv077

Jacob, C., & Melotto, M. (2020). Human pathogen colonization of lettuce dependent upon plant genotype and defense response activation. *Frontiers in Plant Science, 10*, 1769. https://doi.org/10.3389/fpls.2019.01769

Kroupitski, Y., Golberg, D., Belausov, E., Pinto, R., Swartzberg, D., Granot, D., & Sela, S. (2009a). Internalization of Salmonella enterica in leaves is induced by light and involves chemotaxis and penetration through open stomata. *Applied and Environmental Microbiology, 75*(19), 6076–6086. https://doi.org/10.1128/AEM.01084-09. PAGE:STRING:ARTICLE/CHAPTER.

Kroupitski, Y., Pinto, R., Brandl, M. T., Belausov, E., & Sela, S. (2009b). Interactions of Salmonella enterica with lettuce leaves. *Journal of Applied Microbiology, 106*, 1876–1885. https://doi.org/10.1111/j.1365-2672.2009.04152.x

Lenzi, A., Baldi, A., Lombardelli, L., Truschi, S., Marvasi, M., & Bruschi, P. (2022). Contamination of microgreens by Salmonella enterica and Escherichia coli is influenced by selection breeding in chicory (Cichorium intybus L.). *Food Quality and Safety, 6*. https://doi.org/10.1093/fqsafe/fyac030

Ölmez, H. (2016). Foodborne pathogenic bacteria in fresh-cut vegetables and fruits. In P. Kotzekidou (Ed.), *Food hygiene and toxicology in ready-to-eat foods* (pp. 151–166). Academic Press, Elsevier. https://doi.org/10.1016/B978-0-12-801916-0.00009-1.

Lorenzo, J. M., Munekata, P. E., Domínguez, R., Pateiro, M., Saraiva, J. A., & Franco, D. (2018). Main groups of microorganisms of relevance for food safety and stability: General aspects and overall description. In F. J. Barba, M. Koubaa, & P. E. S. Munekata (Eds.), *Innovative technologies for food preservation: Inactivation of spoilage and pathogenic microorganisms* (pp. 53–107). Elsevier. https://doi.org/10.1016/B978-0-12-811031-7.00003-0.

Macarisin, D., Patel, J., Bauchan, G., Giron, J. A., & Ravishankar, S. (2013). Effect of spinach cultivar and bacterial adherence factors on survival of Escherichia coli O157:H7 on spinach leaves. *Journal of Food Protection, 76*(11), 1829–1837. https://doi.org/10.4315/0362-028X.JFP-12-556

Manios, S. G., Konstantinidis, N., Gounadaki, A. S., & Skandamis, P. N. (2013). Dynamics of low (1–4 cells) vs high populations of Listeria monocytogenes and Salmonella typhimurium in fresh-cut salads and their Sterile liquid or solidified extracts. *Food Control, 29*(2), 318–327. https://doi.org/10.1016/J.FOODCONT.2012.04.023

Marshall, K., Hexemer, A., Seelman, S., Fatica, M., Blessington, T., Hajmeer, M., Kisselburgh, H., Atkinson, R., Hill, K., Sharma, D., Needham, M., Peralta, V., Higa, J., Blickenstaff, K., Williams, I., Jhung, M., Wise, M., & Gieraltowski, L. (2020). Lessons learned from a decade of investigations of Shiga toxin–producing Escherichia coli outbreaks linked to leafy greens, United States and Canada. *Emerging Infectious Diseases, 26*, 2319. https://doi.org/10.3201/eid2610.191418

Mir, S. A., Shah, M. A., Mir, M. M., Dar, B. N., Greiner, R., & Roohinejad, S. (2018). Microbiological contamination of ready-to-eat vegetable salads in developing countries and potential solutions in the supply chain to control microbial pathogens. *Food Control, 85*, 235–244. https://doi.org/10.1016/j.foodcont.2017.10.006

Mishra, A., Guo, M., Buchanan, R. L., Schaffner, D. W., & Pradhan, A. K. (2017). Prediction of Escherichia coli O157:H7, Salmonella, and Listeria monocytogenes growth in leafy greens without temperature control. *Journal of Food Protection, 80*(1), 68–73. https://doi.org/10.4315/0362-028X.JFP-16-153

Mishra, A., Roy, S., Shaikh, N. I., Malave, P., Mishra, A., & Alam, M. A. (2024). Recent advances in multiplex aptasensor detection techniques for food-borne pathogens: A comprehensive review of novel approaches. *Biosensors and Bioelectronics X, 16*, Article 100417. https://doi.org/10.1016/j.biosx.2023.100417

Palma-Salgado, S., Ku, K. M., Dong, M., Nguyen, T. H., Juvik, J. A., & Feng, H. (2020). Adhesion and removal of E. coli K12 as affected by leafy green produce epicuticular wax composition, surface roughness, produce and bacterial surface hydrophobicity, and sanitizers. *International Journal of Food Microbiology, 334*, Article 108834. https://doi.org/10.1016/j.ijfoodmicro.2020.108834

Pang, H., Lambertini, E., Buchanan, R. L., Schaffner, D. W., & Pradhan, A. K. (2017). Quantitative microbial risk assessment for Escherichia coli O157:H7 in fresh-cut lettuce. *Journal of Food Protection, 80*(2), 302–311.

Pau, G., Fuchs, F., Sklyar, O., Boutros, M., & Huber, W. (2010). EBImage—an R package for image processing with applications to cellular phenotypes. *Bioinformatics, 26*(7), 979–981. https://doi.org/10.1093/BIOINFORMATICS/BTQ046

Qian, J., Ma, L., Yan, W., Zhuang, H., Huang, M., & Zhang, J. (2022). Inactivation kinetics and cell envelope damages of foodborne pathogens Listeria monocytogenes and Salmonella Enteritidis treated with cold plasma. *Food Microbiology, 101*, Article 103891. https://doi.org/10.1016/j.fm.2021.103891

R Core Team. (2024). *R: A language and environment for statistical computing*. R Foundation for Statistical Computing.

Remus-Emsermann, M. N. P., & Schlechter, R. O. (2018). Phyllosphere microbiology: At the interface between microbial individuals and the plant host. *New Phytologist, 218*(4), 1327–1333. https://doi.org/10.1111/NPH.15054

Roasto, M., Bonardi, S., Mäsaar, M., Alban, L., Gomes-Neves, E., & Vieira-Pinto, M. (2023). Salmonella enterica prevalence, serotype diversity, antimicrobial resistance and control in the European pork production chain. *Trends in Food Science & Technology, 131*, 210–219. https://doi.org/10.1016/j.tifs.2022.12.007

Sant'Ana, A. S., Franco, B. D. G. M., & Schaffner, D. W. (2012). Modeling the growth rate and lag time of different strains of Salmonella enterica and Listeria monocytogenes in ready-to-eat lettuce. *Food Microbiology, 30*(1), 267–273. https://doi.org/10.1016/j.fm.2011.11.003

Seo, K. H., & Frank, J. F. (1999). Attachment of Escherichia coli O157:H7 to lettuce leaf surface and bacterial viability in response to chlorine treatment as demonstrated by using confocal scanning laser microscopy. *Journal of Food Protection, 62*, 3–9. https://doi.org/10.4315/0362-028X-62.1.3

Slayton, R., Turabelidze, G., Bennett, S., Schwensohn, C., Yaffee, A., Khan, F., Butler, C., Trees, E., Ayers, T., & Davis, M. (2013). Outbreak of Shiga toxin–producing Escherichia coli (STEC) O157:H7 associated with romaine lettuce consumption, 2011. *PLoS One, 8*, Article e55300. https://doi.org/10.1371/journal.pone.0055300

Sobhy, M., Ali, S. S., Cui, H., Lin, L., & El-Sapagh, S. (2023). Exploring the potential of 1,8-cineole from cardamom oil against food-borne pathogens: Antibacterial mechanisms and its application in meat preservation. *Microbial Pathogenesis, 184*, Article 106375. https://doi.org/10.1016/j.micpath.2023.106375

Taylor, E. V., Nguyen, T. A., Machesky, K. D., Koch, E., Sotir, M. J., Bohm, S. R., Folster, P., Bokanyi, R., Kupper, A., & Bidol, S. A. (2013). Multistate outbreak of Escherichia coli O145 infections associated with romaine lettuce consumption, 2010. *Journal of Food Protection, 76*, 939–944. https://doi.org/10.4315/0362-028X.JFP-12-503

Truschi, S., Baldi, A., Bruschi, P., Cacciari, I., Marvasi, M., & Lenzi, A. (2023). Foliar roughness and water content impact on Escherichia coli attachment in baby leafy greens. *Biology, 12*, 102. https://doi.org/10.3390/biology12010102

Truschi, S., Marini, L., Cacciari, I., Baldi, A., Bruschi, P., Lenzi, A., Baales, J., Zeisler-Diehl, V. V., Schreiber, L., & Marvasi, M. (2024). Relationship between Salmonella enterica attachment and leaf hydrophobicity, roughness, and epicuticular waxes: A focus on 30 baby-leaf salads. *Journal of the Science of Food and Agriculture, 104*, 9287–9296. https://doi.org/10.1002/jsfa.13751

Venables, W. N., & Ripley, B. D. (2002). *Modern applied statistics with S* (4th ed.). New York: Springer. https://doi.org/10.1007/978-0-387-21706-2

Waltenburg, M. A., Schwensohn, C., Madad, A., Seelman, S. L., Peralta, V., Koske, S. E., Boyle, M. M., Arends, K., Patel, K., & Mattioli, M. (2022). Two multistate outbreaks of a reoccurring Shiga toxin–producing Escherichia coli strain associated with romaine lettuce: USA, 2018–2019. *Epidemiology and Infection, 150*, E16. https://doi.org/10.1017/S0950268821002703

Wang, K., Kang, L., Anand, A., Lazarovits, G., & Mysore, K. S. (2007). Monitoring in planta bacterial infection at both cellular and whole-plant levels using the green fluorescent protein variant GFPuv. *New Phytologist, 174*(1), 212–223. https://doi.org/10.1111/j.1469-8137.2007.01999.x

Wickham, H., François, R., Henry, L., Müller, K., & Vaughan, D. (2023). *Dplyr: A grammar of data manipulation*.

Wickham, H., & Girlich, M. (2023). *Tidyr: Tidy messy data*.

Wilson, E., Okuom, M., Kyes, N., Mayfield, D., Wilson, C., Sabatka, D., Sandoval, J., Foote, J. R., Kangas, M. J., Holmes, A. E., & Sutlief, A. L. (2018). Using fluorescence intensity of enhanced green fluorescent protein to quantify Pseudomonas aeruginosa. *Chemosensors, 6*(2), 21. https://doi.org/10.3390/chemosensors6020021

Wood, S. N. (2017). Generalized additive models: An introduction with R. In *Generalized additive models: An introduction with R* (2nd ed., pp. 1–476). https://doi.org/10.1201/9781315370279/GENERALIZED-ADDITIVE-MODELS-SIMON-WOOD/RIGHTS-AND-PERMISSIONS

Wood, S. N. (2024). *Mgcv: Mixed GAM computation vehicle with automatic smoothness estimation*.

Yuan, J., Wang, X., Zhou, H., Li, Y., Zhang, J., Yu, S., Wang, M., Hao, M., Zhao, Q., Liu, L., Li, M., & Li, J. (2020). Comparison of sample preparation techniques for inspection of leaf epidermises using light microscopy and scanning electronic microscopy. *Frontiers in Plant Science, 11*, Article 492104. https://doi.org/10.3389/FPLS.2020.00133/TEXT

Zhou, B., Luo, Y., Bauchan, G. R., Feng, H., & Stommel, J. R. (2018). Visualizing pathogen internalization pathways in fresh tomatoes using MicroCT and confocal laser scanning microscopy *. *Food Control, 85*, 276–282. https://doi.org/10.1016/j.foodcont.2017.09.027